

# Current-Driven Domain-Wall Dynamics in Curved Ferromagnetic Nanowires

Benjamin Krüger and Daniela Pfannkuche

*I. Institut für Theoretische Physik, Universität Hamburg, Jungiusstr. 9, 20355 Hamburg, Germany*

Markus Bolte, Guido Meier, and Ulrich Merkt

*Institut für Angewandte Physik und Zentrum für Mikrostrukturforschung,  
Universität Hamburg, Jungiusstr. 11, 20355 Hamburg, Germany*

(Dated: July 8, 2021)

The current-induced motion of a domain wall in a semicircle nanowire with applied Zeeman field is investigated. Starting from a micromagnetic model we derive an analytical solution which characterizes the domain-wall motion as a harmonic oscillation. This solution relates the micromagnetic material parameters with the dynamical characteristics of a harmonic oscillator, i.e., domain-wall mass, resonance frequency, damping constant, and force acting on the wall. For wires with strong curvature the dipole moment of the wall as well as its geometry influence the eigenmodes of the oscillator. Based on these results we suggest experiments for the determination of material parameters which otherwise are difficult to access. Numerical calculations confirm our analytical solution and show its limitations.

PACS numbers: 75.60.Ch, 72.25.Ba, 76.50.+g

## I. INTRODUCTION

Field-driven dynamics of magnetic domain walls have been intensely studied over the last decades.<sup>1,2</sup> The topic has recently regained interest by the discovery that spin-polarized currents of high density can alter magnetization configurations<sup>3,4,5,6</sup> and move domain walls.<sup>7,8,9,10,11</sup> Current-induced magnetic switching is viewed as a promising solution for the realization of magnetic random access memories<sup>6,12,13</sup>, while current-induced domain-wall motion has potential application in spintronic data storage devices, e.g. in the race-track memory<sup>14</sup> or data transfer schemes.<sup>15,16,17</sup> Several models of current-driven magnetization dynamics have been established to explain the electronic origin of current-induced magnetization changes and to predict their effects.<sup>3,4,18,19,20,21</sup> At first it was assumed that for finite domain walls the spins of the conduction electrons adiabatically follow the local magnetic moments.<sup>18,22</sup> Later the theoretical model was extended to include a non-adiabatic mismatch between the current polarization and the direction of magnetization.<sup>19,20,21</sup>

The measured and calculated velocities of current-driven magnetic domain walls in thin nanowires vary by several orders of magnitude even for the same material.<sup>7,21,23,24,25</sup> While it has been originally suggested that the discrepancy could be due to thermal activation<sup>11,25,26,27,28</sup> or surface roughness<sup>25</sup>, it has recently been found that the domain-wall velocity depends on the type of the domain wall<sup>26,29</sup> which can be changed by a spin-polarized current.<sup>8,26,30,31</sup> Recently it has been observed that the velocity of field-driven domain-wall motion<sup>32</sup> can be altered by  $\pm 100$  m/s by a pulsed spin-polarized current<sup>33</sup> and that the motion can even be halted completely.<sup>34</sup> It is now assumed that the adiabatic term is largely responsible for the acceleration of the domain wall while the non-adiabatic term will cause

the wall to continually move.<sup>21</sup> It has been shown that domain-wall oscillations excited with an ac current at its resonance frequency require current densities one to two orders of magnitude less ( $10^{10}$  A/m<sup>2</sup>, see Ref.<sup>9,35</sup>) than for pulsed excitations ( $10^{11}$ – $10^{12}$  A/m<sup>2</sup>, see Ref.<sup>6,7,11,26</sup>).

Here we show that the harmonic-oscillator model follows naturally from a micromagnetic model that describes the excitation of transverse walls in thin narrow rings.<sup>36,37,38</sup> Solving analytically the Landau-Lifshitz-Gilbert equation extended by the current corrections due to Zhang and Li<sup>21</sup> we are able to express the properties of the driven oscillator by the quantities determining the micromagnetic model. A comparison of the numerical calculations with our analytical solution confirms the importance of the geometry due to the curved wires. Finally, we suggest experiments which can determine the values of the non-adiabatic spin torque and the Gilbert damping parameter.

## II. MODEL

Figure 1 shows a ferromagnetic semicircle nanowire with a domain wall at its bottom placed in an external magnetic field.<sup>39</sup> The wall is excited by an oscillating current flowing between the two contacts.<sup>9</sup>

The magnetization dynamics of a magnetic wire is well described by the Landau-Lifshitz-Gilbert (LLG) equation.<sup>40</sup> In the presence of a spin-polarized current density  $\vec{j}$ , the interaction between the itinerant electrons and the magnetization  $\vec{M}$  leads to an extension of the LLG equation. This extension was derived from a quantum mechanical model by Zhang and Li.<sup>21</sup> Their semiclassical approximation results in the extended LLG

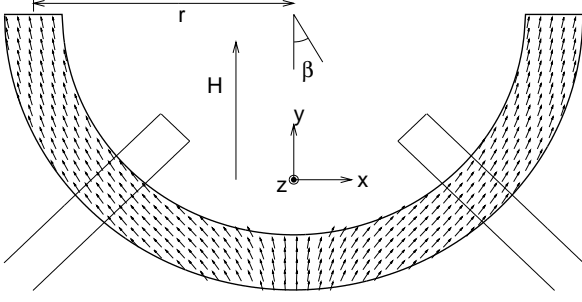


FIG. 1: Scheme of the semicircle nanowire with radius  $r$  in a magnetic field  $H$ . The static magnetization in the absence of a current is indicated by small arrows. The two rectangles under angles  $\beta = \pm 45^\circ$  are the electrical contacts.

equation (in Gilbert form)

$$\begin{aligned} \frac{d\vec{M}}{dt} = & -\gamma\vec{M} \times \vec{H}_{\text{eff}} + \frac{\alpha}{M_s}\vec{M} \times \frac{d\vec{M}}{dt} \\ & - \frac{b_j}{M_s^2}\vec{M} \times (\vec{M} \times (\vec{j} \cdot \vec{\nabla})\vec{M}) \\ & - \xi \frac{b_j}{M_s}\vec{M} \times (\vec{j} \cdot \vec{\nabla})\vec{M} \end{aligned} \quad (1)$$

with the gyromagnetic ratio  $\gamma$ , the Gilbert damping parameter  $\alpha$ , the saturation magnetization  $M_s$ , and the ratio between exchange relaxation time and spin-flip relaxation time  $\xi = \tau_{\text{ex}}/\tau_{\text{sf}}$ . The effective magnetic field  $H_{\text{eff}}$  includes the external as well as the internal fields. In this model the spin current is sensitive to the spatial inhomogeneities of the magnetization with a coupling constant  $b_j = \frac{P\mu_B}{eM_s(1+\xi^2)}$  where  $P$  denotes the spin polarization of the current and  $\mu_B$  is the Bohr magneton.

Since the saturation magnetization is constant for a given material at fixed temperature,  $\vec{M}$  is perpendicular to  $\frac{d\vec{M}}{dt}$  and Eq. (1) can be reformulated to an explicit equation of motion for the magnetization

$$\begin{aligned} \frac{d\vec{M}}{dt} = & -\gamma'\vec{M} \times \vec{H}_{\text{eff}} - \frac{\alpha\gamma'}{M_s}\vec{M} \times (\vec{M} \times \vec{H}_{\text{eff}}) \\ & - \frac{b'_j}{M_s^2}(1 + \alpha\xi)\vec{M} \times (\vec{M} \times (\vec{j} \cdot \vec{\nabla})\vec{M}) \\ & - \frac{b'_j}{M_s}(\xi - \alpha)\vec{M} \times (\vec{j} \cdot \vec{\nabla})\vec{M} \end{aligned} \quad (2)$$

with the abbreviations  $\gamma' = \frac{\gamma}{1+\alpha^2}$  and  $b'_j = \frac{b_j}{1+\alpha^2}$ . This equation is the starting point for the analytical as well as for the numerical calculations presented in the following.

### III. ANALYTICAL CALCULATIONS OF THE STRAIGHT WIRE

For the analytical treatment of Eq. (2) we transform the semicircle wire in a homogeneous Zeeman field to

a straight wire in a spatially varying field. The wire is directed along the  $x$ -axis. The direction of the magnetization will be expressed in a polar spin basis  $\vec{M} = M_s(\cos\theta, \sin\theta \cos\phi, \sin\theta \sin\phi)$ . In the absence of electric current and external magnetic field the energy of a domain wall within the wire is

$$E = S \int \left[ A \left( \frac{\partial\theta(x)}{\partial x} \right)^2 + K \sin^2\theta(x) \right] dx, \quad (3)$$

where  $\theta$  denotes the angle between the wire axis and the magnetization.  $A$  and  $K$  denote the exchange and the shape anisotropy constant. This functional can be minimized by the well known Néel wall described by the angle

$$\theta = \pi - 2 \arctan \left( e^{\frac{x-X}{\lambda}} \right). \quad (4)$$

The center of the wall is at position  $X$  and the width of the domain wall is  $\lambda = \sqrt{A/K}$ . From Eq. (4) two expressions

$$\cos\theta = \tanh \left( \frac{x-X}{\lambda} \right), \quad \sin\theta = \frac{1}{\cosh \left( \frac{x-X}{\lambda} \right)} \quad (5)$$

can be derived which will be useful in our further calculations.

In the presence of an external field  $H_{\text{ext}}$  the demagnetization energy  $K_{\perp} \sin^2\theta \sin^2\phi$  caused by the rotation of the wall around the wire axis can no longer be neglected. We include the external field perpendicular to the wire into the shape anisotropy  $K_{\perp}$ . The energy functional in Eq. (3) has to be extended to

$$\begin{aligned} E = & \int \left[ K \sin^2\theta + A \left( \frac{\partial\theta}{\partial x} \right)^2 \right] dV \\ & + \int [K_{\perp} \sin^2\theta \sin^2\phi - \mu_0 M_s H_{\text{ext}}(x) \cos\theta] dV. \end{aligned} \quad (6)$$

Here we have restricted ourselves to an external field parallel to the wire. Also the crystalline anisotropy has been neglected.<sup>41</sup> From the energy functional in Eq. (6) we derive the effective magnetic field through the relation  $\vec{H}_{\text{eff}} = -\frac{1}{\mu_0} \frac{\delta E}{\delta \vec{M}}$ .

From the extended LLG equation (2) in the polar spin basis we obtain

$$\begin{aligned} \dot{\theta} = & -\frac{\gamma'}{\mu_0 M_s \sin(\theta)} \frac{\delta E}{\delta \phi} - \frac{\gamma' \alpha}{\mu_0 M_s} \frac{\delta E}{\delta \theta} \\ & + b'_j(1 + \alpha\xi)\vec{j} \cdot \vec{\nabla}\theta + b'_j(\xi - \alpha)\sin(\theta)\vec{j} \cdot \vec{\nabla}\phi \end{aligned} \quad (7)$$

and

$$\begin{aligned} \dot{\phi} \sin\theta = & \frac{\gamma'}{\mu_0 M_s} \frac{\delta E}{\delta \theta} - \frac{\gamma' \alpha}{\mu_0 M_s \sin(\theta)} \frac{\delta E}{\delta \phi} \\ & + \sin(\theta)b'_j(1 + \alpha\xi)\vec{j} \cdot \vec{\nabla}\phi - b'_j(\xi - \alpha)\vec{j} \cdot \vec{\nabla}\theta. \end{aligned} \quad (8)$$

Assuming that the moving wall stays a Néel wall we can describe its motion, following the description of

Schreyer and Walker<sup>2</sup>, by two dynamical variables: the position of its center  $X$  and its angle around the wire axis  $\phi(x) = \phi$  that is uniform along the wire. With Eq. (5) and Eq. (6) we get from Eq. (7) and Eq. (8)

$$\begin{aligned} \frac{\sin(\theta)}{\lambda} \dot{X} &= -\frac{2K_{\perp}\gamma'}{\mu_0 M_s} \sin(\theta) \sin(\phi) \cos(\phi) \\ &\quad - \alpha\gamma' \sin(\theta) H_{\text{ext}}(x) - \frac{b'_j}{\lambda} \sin(\theta)(1 + \alpha\xi)j \\ &\quad - \frac{2K_{\perp}\gamma'\alpha}{\mu_0 M_s} \sin(\theta) \cos(\theta) \sin^2(\phi) \end{aligned} \quad (9)$$

and

$$\begin{aligned} \dot{\phi} \sin \theta &= \sin(\theta)\gamma' H_{\text{ext}}(x) + \sin(\theta) \frac{b'_j(\xi - \alpha)j}{\lambda} \\ &\quad - 2 \sin(\theta)\gamma'\alpha K_{\perp} \sin(\phi) \cos(\phi) \frac{1}{\mu_0 M_s} \\ &\quad + \frac{2K_{\perp}\gamma'}{\mu_0 M_s} \sin(\theta) \cos(\theta) \sin^2(\phi). \end{aligned} \quad (10)$$

Note, that  $X$  and  $\phi$  depend on the position  $x$  along the wire. In the following we show that a solution consistent with our initial assumptions exists for small excitations.<sup>2</sup> Note, that this condition holds for realistic current densities.

Assuming that  $H_{\text{ext}}(x)$  varies slowly on the length scale of the domain-wall width  $\lambda = \sqrt{A/K}$ ,  $\sin \theta$  is replaced by a  $\delta$ -function  $\pi\lambda\delta(x - X)$  in view of Eq. (5). Also we neglect terms which are nonlinear in  $\phi$ . This approximation holds for angles  $\phi$  smaller than about  $10^\circ$ .

The equations of motion for the domain wall then become

$$\dot{X} = -\lambda 2\gamma' K_{\perp} \phi \frac{1}{\mu_0 M_s} - \lambda\gamma'\alpha H_{\text{ext}}(X) - b'_j(1 + \alpha\xi)j \quad (11)$$

and

$$\dot{\phi} = \gamma' H_{\text{ext}}(X) - 2\gamma'\alpha K_{\perp} \phi \frac{1}{\mu_0 M_s} + \frac{b'_j(\xi - \alpha)j}{\lambda}. \quad (12)$$

These equations are general equations of motion with a time dependent current density  $j$ .

In the limit of a steady current and a homogeneous magnetic field one can calculate the initial velocity of the wall by setting  $\dot{\phi} = 0$ , the initial condition of the Néel wall. This leads to the initial velocity  $\dot{X}_i = -\lambda\gamma'\alpha H_{\text{ext}} - b'_j(1 + \alpha\xi)j$  which is exactly the value obtained by Zhang and Li.<sup>21</sup> The terminal velocity  $\dot{X}_f = -(\lambda\gamma' H_{\text{ext}} + b'_j \xi j) / \alpha$  is calculated by setting  $\dot{\phi} = 0$ , i.e., stationary motion. This velocity is also identical to the one calculated by Zhang and Li. Similar relations have recently been found by Dugaev et al.<sup>42</sup>

The domain-wall mass is obtained by determining  $\sin \phi$  in the absence of electric currents and external fields. From Eq. (11) we obtain for the stationary motion

$$\phi = -\dot{X} \frac{\mu_0 M_s}{2\lambda\gamma' K_{\perp}}. \quad (13)$$

Inserting this result into the  $\phi$ -dependent part of the domain-wall energy in Eq. (6) and comparing with the energy  $E$  of the domain-wall quasiparticle

$$\begin{aligned} \frac{1}{2} m \dot{X}^2 &= E \\ &= S \int dx K_{\perp} \sin^2(\theta) \left( \dot{X} \frac{\mu_0 M_s}{\lambda 2\gamma' K_{\perp}} \right)^2 \\ &= \frac{1}{2} \frac{S \mu_0^2 M_s^2}{\lambda \gamma'^2 K_{\perp}} \dot{X}^2 \end{aligned} \quad (14)$$

we arrive at the domain-wall mass

$$m = \frac{S \mu_0^2 M_s^2}{\lambda \gamma'^2 K_{\perp}}. \quad (15)$$

Note that this result relates the phenomenological domain-wall mass of a tail-to-tail Néel wall to the micromagnetic material parameters.

In the case of a curved wire the projection of a uniform external field along the wire is given by  $H_{\text{ext}}(x) = H_0 \sin(x/r)$ . Transferring this to our straight wire model, at small displacements of the domain wall ( $X \ll r$ ) the wall is exposed to the external field  $H_{\text{ext}} \approx H_0 X/r$ . Then the equations of motion become a system of two coupled linear differential equations of first order:

$$\begin{pmatrix} \dot{X} \\ \dot{\phi} \end{pmatrix} = \gamma' \begin{pmatrix} -\lambda\alpha H_0 \frac{1}{r} & -\lambda 2K_{\perp} \frac{1}{\mu_0 M_s} \\ H_0 \frac{1}{r} & -2\alpha K_{\perp} \frac{1}{\mu_0 M_s} \end{pmatrix} \begin{pmatrix} X \\ \phi \end{pmatrix} + b'_j j \begin{pmatrix} -(1 + \alpha\xi) \\ \frac{(\xi - \alpha)}{\lambda} \end{pmatrix}. \quad (16)$$

Except for the non-vanishing first matrix element  $-\lambda\alpha H_0/r$  these equations are equivalent to those of a driven harmonic oscillator. For a time dependent current density of the form  $j_0 e^{i\Omega t}$  the general solution

$$\begin{pmatrix} X(t) \\ \phi(t) \end{pmatrix} = \begin{pmatrix} X_+ \\ \phi_+ \end{pmatrix} e^{-\Gamma t + i\omega_f t} + \begin{pmatrix} X_- \\ \phi_- \end{pmatrix} e^{-\Gamma t - i\omega_f t} + \frac{1}{\omega_r^2 - \Omega^2 + 2i\Omega\Gamma} \frac{F}{m} \quad (17)$$

consists of an exponentially damped starting configuration with the initial conditions described by  $X_{\pm}$  and  $\phi_{\pm}$  and a current-driven oscillation with the driving force  $\vec{F}$ . The damping constant

$$\Gamma = \alpha\gamma' \left( \frac{\lambda H_0}{2r} + \frac{K_{\perp}}{\mu_0 M_s} \right) \quad (18)$$

depends on the ratio of applied magnetic field and ring radius. It represents the restoring force acting on the domain wall. This dependence of the damping constant on the restoring force expresses that the damping is spatially dependent. This also leads to a second term in the frequency of the free oscillation

$$\omega_f = \sqrt{\frac{2\gamma'^2 H_0 \lambda K_{\perp}}{\mu_0 M_s r} - \alpha^2 \gamma'^2 \left( \frac{K_{\perp}}{\mu_0 M_s} - \frac{\lambda H_0}{2r} \right)^2} \quad (19)$$

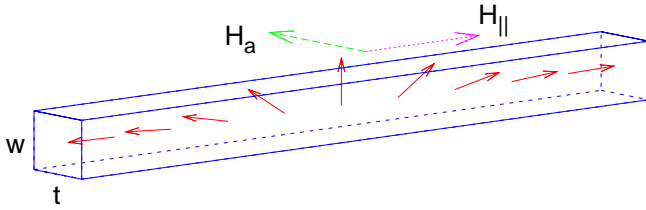


FIG. 2: (Color online) Schematic illustration of the magnetization in the Néel wall (solid red arrows) in a straight wire of width  $w$  and thickness  $t$ .  $H_{\parallel}$  and  $H_a$  are the parallel component of the external field and the anisotropy field, respectively.

which is different from  $\Gamma$ . Hence the resonance frequency

$$\omega_r = \sqrt{\omega_f^2 + \Gamma^2} = \sqrt{\frac{2\gamma'^2 H_0 \lambda K_{\perp}}{\mu_0 M_s r} (1 + \alpha^2)} \quad (20)$$

depends explicitly on the Gilbert damping  $\alpha$  and differs from the resonance frequency of a normal harmonic oscillator

$$\omega_0 = \sqrt{\frac{D}{m}} = \sqrt{\frac{2\gamma'^2 H_0 \lambda K_{\perp}}{\mu_0 M_s r}} \quad (21)$$

by the factor  $\sqrt{1 + \alpha^2}$ . The constant  $D$  is given by  $D = F_H/X$  where  $F_H$  is the force on the domain wall due to the external magnetic field. The force

$$\begin{aligned} \vec{F} = & -mb_j j_0 e^{i\Omega t} \left( \frac{2\gamma' K_{\perp} \xi}{\mu_0 M_s} + \frac{1 + \alpha \xi}{1 + \alpha^2} i\Omega \right) \vec{e}_X \\ & - mb_j j_0 e^{i\Omega t} \left( \gamma' H_0 \frac{1}{r} - \frac{\xi - \alpha}{1 + \alpha^2} \frac{i\Omega}{\lambda} \right) \vec{e}_{\phi} \end{aligned} \quad (22)$$

induced by the current depends on the frequency  $\Omega$  of the applied current.

The terms in Eq. (22) can be understood as direct forces due to the spin torque and the precessions of the magnetization in the external and anisotropy field depicted in Fig. 2. The terms proportional to  $i\Omega$  express the current-induced spin torque. They are the time derivatives of the inhomogeneities in Eq. (16). The  $H_0$ -dependent term is a result of the precession of the magnetization in the external field which causes a rotation of the wall around the wire axis. The precession in the anisotropy field, described by the  $K_{\perp}$ -term in Eq. (22), causes a change of the wall velocity.

Except that the force depends on the frequency  $\Omega$  of the applied current the result for the domain wall displacement is equal to the one in a harmonic oscillator. With increasing  $\Omega$  the force increases and its phase shifts up to  $90^\circ$ . In the absence of a non-adiabatic spin torque ( $\xi = 0$ ) current and domain-wall displacement at resonance have opposite sign. In case of a non-adiabatic

torque the phase at resonance frequency between the current and the magnetization in  $z$ -direction is  $90^\circ$  when the ratio  $\xi$  of exchange and spin-flip relaxation time equals the Gilbert damping parameter ( $\xi = \alpha$ ). The phase can be used to find out whether a non-adiabatic spin torque exists and to determine the value of  $\xi$  in comparison to the damping parameter  $\alpha$ .

The influence of the adiabatic torque on the position of the wall is obtained by setting  $\xi = 0$  in Eq. (22). The  $x$ -component of the force  $\vec{F}$  due to the adiabatic torque is proportional to the time derivative of the current density. Therefore, the adiabatic torque does not accelerate the wall when the current does not change in time. This explains the observation of Zhang and Li<sup>21</sup> that without a non-adiabatic spin torque a domain wall subjected to a steady current stops moving. In contrast the non-adiabatic contributions to the force are proportional to the current density as well as to its derivative.

In Eq. (17) the starting configuration depends on  $\phi_{\pm}$  and  $X_{\pm}$ . The equation that follows from decoupling of Eq. (16)

$$\phi_{\pm} = \left( \frac{\alpha}{2\lambda} - \frac{\alpha H_0 \mu_0 M_s}{4r K_{\perp}} \pm i \frac{\omega_f \mu_0 M_s}{2\lambda \gamma' K_{\perp}} \right) X_{\pm} \quad (23)$$

connects  $\phi_{\pm}$  with  $X_{\pm}$ . Hence we have two parameters left for our starting configuration as expected for an oscillation.

With the above analytical model we are able to derive the hitherto phenomenological oscillator model<sup>9</sup> and to express its characteristics by the micromagnetic material parameters. Likewise, the measurement of the domain-wall motion allows the determination of micromagnetic quantities.

#### IV. CURVED WIRES

For curved wires in a homogeneous magnetic field its component perpendicular to the wire has to be taken into account. Also the change of the magnetization due to the curvature becomes important. To include the perpendicular field we calculate the force on the domain wall as the spatial derivative of its Zeeman energy. The total magnetic moments parallel to the wire

$$m_{\parallel} = \int M_s \cos[\theta(x)] dV = -2M_s S X \quad (24)$$

and perpendicular to the wire

$$m_{\perp} = \int M_s \sin[\theta(x)] dV = \pi M_s S \lambda \quad (25)$$

are volume integrals over its magnetization that are readily calculated using the relations in Eq. (5). Note that  $m_{\parallel}$  is the magnetic moment of an abrupt domain wall. With the magnetic field  $H_0$  in  $y$ -direction the Zeeman

energy can be written as

$$E_{\parallel} = \mu_0 M_s H t \int_{r-\frac{w}{2}}^{r+\frac{w}{2}} r' \left[ \int_{-\frac{\pi}{2}}^{\beta_0} \sin(\beta) d\beta - \int_{\beta_0}^{\frac{\pi}{2}} \sin(\beta) d\beta \right] dr' \quad (26)$$

where  $\beta_0 = \frac{X}{r}$  is the angle of the position of the domain wall (see Fig. 1) and  $r$ ,  $w$ , and  $t$  are the radius, the width, and the thickness of the wire. We get

$$E_{\parallel} = -2\mu_0 M_s S r H \cos(\beta_0) = 2\mu_0 M_s S H Y \quad (27)$$

with the cross section  $S = wt$ . One recognizes that the energy is equivalent to the energy of a monopole with magnetic charge  $Q_M = 2\mu_0 M_s S$ . For small domain-wall displacements we can write the cosine in Eq. (27) as a Taylor series up to second order in  $X$  and get

$$E_{\parallel} \approx -2\mu_0 M_s S r H \left( 1 - \frac{X^2}{2r^2} \right). \quad (28)$$

The monopole has been included in the above calculations as well as in the calculations of Saitoh et al.<sup>9</sup> The perpendicular magnetization contributes to the Zeeman energy

$$E_{\perp} = -\mu_0 m_{\perp} H \cos\left(\frac{X}{r}\right) \approx -P_M H \left( 1 - \frac{X^2}{2r^2} \right) \quad (29)$$

and can be interpreted as the energy of a magnetic dipole with moment  $P_M = \mu_0 \pi M_s S \lambda$ . The Zeeman energy of the perpendicular magnetization has previously not been included in the magnetic energy. It gives a correction to the magnetic force on the domain wall,

$$\begin{aligned} F_x &= -\frac{dE}{dX} \approx -\frac{2\mu_0 M_s S H}{r} X - \frac{\pi\mu_0 M_s S \lambda H}{r^2} X \\ &= -\frac{Q_M H}{r} X - \frac{P_M H}{r^2} X = -\frac{Q_M}{r} X H \left( 1 + \frac{\pi\lambda}{2r} \right). \end{aligned} \quad (30)$$

Thus, we include the action of a field component perpendicular to the wire by replacing the field in Eq. (17) by an effective field  $H_{\text{eff}} = H (1 + P_M/Q_M r)$ .

We now take into account the curvature of the wire. With decreasing ring radius the angle between neighboring spins in the domain wall shrinks. This leads to an additional contribution to the exchange energy of the wall when its magnetization points out of the wire plane.

To calculate the new exchange energy we change the spin basis to Cartesian coordinates. To distinguish the spin basis from the basis in space we introduce the coordinates  $\chi = \cos\theta$ ,  $\eta = \sin\theta \cos\phi$ , and  $\zeta = \sin\theta \sin\phi$ . Moving along the wire the magnetization performs a rotation in  $-\theta$  direction due to the domain wall as well as a rotation around the  $\zeta$  axis due to the curvature. For small rotations  $\Delta\theta$  and  $\Delta\beta$  the Cartesian coordinates are

given by

$$\begin{aligned} \chi &= \cos(\Delta\beta) \cos(\theta + \Delta\theta) - \sin(\Delta\beta) \sin(\theta + \Delta\theta) \cos(\phi) \\ \eta &= \cos(\Delta\beta) \sin(\theta + \Delta\theta) \cos(\phi) + \sin(\Delta\beta) \cos(\theta + \Delta\theta) \\ \zeta &= \sin(\theta + \Delta\theta) \sin(\phi). \end{aligned} \quad (31)$$

The exchange energy density is given by

$$W_{\text{ex}} = A \left[ \left( \frac{\partial\chi}{\partial x} \right)^2 + \left( \frac{\partial\eta}{\partial x} \right)^2 + \left( \frac{\partial\zeta}{\partial x} \right)^2 \right]. \quad (32)$$

From Eq. (31) we obtain

$$\begin{aligned} W_{\text{ex}} &= A \left( \frac{\partial\theta}{\partial x} \right)^2 + 2A \frac{\partial\theta}{\partial x} \frac{1}{r} \cos\phi \\ &\quad - A \frac{1}{r^2} \sin^2\theta \sin^2\phi + \frac{A}{r^2}. \end{aligned} \quad (33)$$

The first term is equal to the exchange energy density of the straight wire. The last term is constant and does not depend on the magnetization. In the approximation for small  $\phi$  the other two terms can be rewritten

$$\Delta W_{\text{ex}} = A \frac{\partial\theta}{\partial x} \frac{1}{r} (2 - \phi^2) - A \left( \frac{\phi}{r} \right)^2 \sin^2\theta. \quad (34)$$

Integration leads to the contribution

$$\int dV \Delta W_{\text{ex}} = \left( \frac{AS\pi}{r} - \frac{AS2\lambda}{r^2} \right) \phi^2 - \frac{2AS\pi}{r} \quad (35)$$

of the curvature to the anisotropy energy. The last term is a constant which does not depend on  $X$  or  $\phi$ . The perpendicular anisotropy energy can be written as

$$\int dV W_{\text{a}\perp} = \int dV K_{\perp} \sin^2\theta \sin^2\phi = K_{\perp} S 2\lambda \phi^2. \quad (36)$$

Comparing Eqs. (35) and (36) one can see that the additional exchange energy due to the curvature can be included into the perpendicular anisotropy by defining an effective anisotropy constant

$$K_{\perp\text{eff}} = K_{\perp} + \frac{A\pi}{2\lambda r} - \frac{A}{r^2}. \quad (37)$$

## V. NUMERICAL CALCULATIONS

To check the applicability of the approximations made in our analytical model, i.e. the form invariance of the domain wall at small displacements, we have performed micromagnetic simulations. We have modelled current induced domain-wall oscillations in curved nanowires as described in Sec. II. The current contacts are arranged under an angle of  $90^\circ$  to have sufficient distance to the domain wall as well as to the ends of the wire (see Fig. 1).

We extended the implementation of the Landau-Lifshitz-Gilbert-equation in the Object Oriented Micro Magnetic Framework (OOMMF)<sup>43</sup> by the additional current-dependent terms of Eq. (2) and implemented Runge-Kutta and Adams-Bashforth-Moulton algorithms of higher order to speed up the calculations. The calculations presented here have been performed using the explicit embedded Runge-Kutta 5(4) algorithm by Cash and Karp.<sup>44</sup> The current density is calculated by locally solving Ohm's law, thus taking the curvature of the wire and the contacts into account. For the spatial discretization a cell size of 1 nm in  $x$ - and  $y$ -direction and 10 nm in  $z$ -direction was chosen. Numerical calculations were performed for radii of 45 nm, 55 nm, 65 nm, 70 nm, 85 nm, and 95 nm with different polarized current densities  $j_p = jP$ . We use the material parameters of permalloy, i.e. the exchange constant  $A = 13 \cdot 10^{-12}$  J/m and the saturation magnetization  $M_s = 8 \cdot 10^5$  A/m. All wires have a quadratical cross section  $S = wt = 100$  nm<sup>2</sup>. The applied field in  $y$ -direction was chosen to be 125 mT to increase the resonance frequency, see Eq. (20), and thus to reduce the simulation time necessary for the domain wall to perform several oscillations. Due to the small width of the wire this high field has virtually no effect on the ground state ( $H = 0$ ) of the magnetization. In the ground state we obtain a domain-wall width of  $\lambda = 9.25$  nm. The difference in the magnetization orientation  $\theta$  between the analytical description of the Néel wall and the micromagnetic ground state in the curved wire is less than  $5^\circ$ .

We have determined the eigenmodes of the magnetization in the wire by applying a magnetic  $\delta$ -pulse in  $z$ -direction (see Fig. 1), thus exciting all frequencies with equal amplitude. To mimic an applied current, the magnetic field pulse has been chosen to point in  $z$ -direction so that the torque of the field points in the same direction as the torque of the applied current [see Eq. (2)]. After this excitation the system performs damped free oscillations. The eigenmodes of the wire are found by spatially resolved discrete Fourier transformation (see Fig. 3).<sup>45,46</sup> The higher harmonics and the standing spin waves in the wire are neglected in the analytical description. The resonance of the ground mode is observed at a frequency of  $\Omega = 15.7$  GHz. The higher modes are also indicated in Fig. 3. However in the following we focus on the ground mode.

We simulated an alternating current with frequencies close to the resonance frequency of the domain wall for different radii  $r$  and Gilbert damping parameters  $\alpha$ . Figure 4 shows the numerically obtained amplitudes for different radii at fixed  $\alpha = 0.05$  and  $\xi = 0.01$ . For each radius the position and the width of the resonance curve have been fitted to the analytical model, Eq. (17), to determine the parameters  $F(r)$ ,  $\omega_r(r)$ , and  $\Gamma(r)$ . Note that all resonance curves are in excellent agreement with the harmonic-oscillator model. The frequencies  $\omega_r(r)$  and the damping constants  $\Gamma(r)$  have been summarized in Fig. 5 where they are compared to the analytical expres-

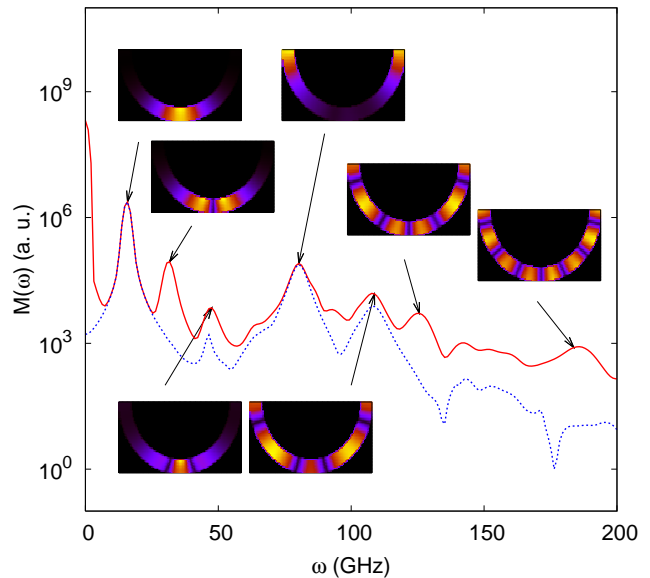


FIG. 3: (Color online) Fourier transform  $M(\omega)$  of the simulated magnetization  $M_x(t)$  in a curved nanowire with radius  $r = 45$  nm and Gilbert damping parameter  $\alpha = 0.05$ . The wire is excited with a magnetic  $\delta$ -pulse. The lines show the spatially resolved (solid line) and the integral response (dashed line). The insets show the spatially resolved discrete Fourier transforms for seven selected eigenfrequencies.

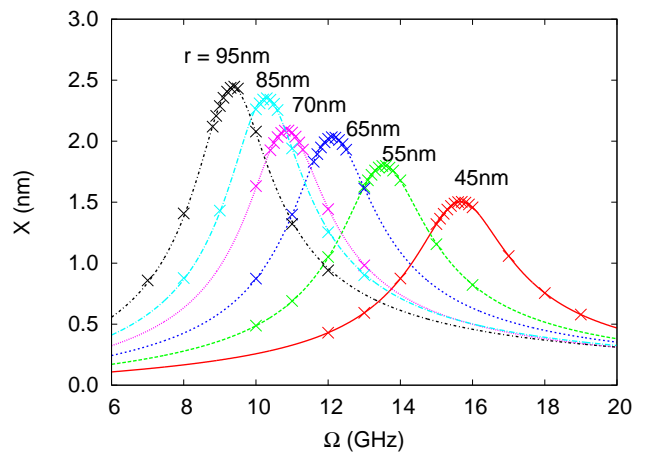


FIG. 4: (Color online) Amplitude of the domain-wall displacement versus frequency of the applied current for different radii  $r$ . The Gilbert damping  $\alpha = 0.05$ , the ratio of the exchange and spin-flip relaxation time  $\xi = 0.01$ , and the polarized current density  $j_p = 10^{11}$  A/m<sup>2</sup> are fixed. The crosses denote numerical values while the lines are fits with the analytical result of Eq. (17).

sions in Eq. (18) and Eq. (20). The results coincide if we assume  $K_{\perp\text{eff}} = K_{\perp} + \frac{A\pi}{2\lambda r} - \frac{A}{r^2}$  with  $K_{\perp} = 60000$  J/m<sup>3</sup> for the perpendicular anisotropy [see Eq. (37)]. The dependence of the resonance frequency  $\omega_r$  on the radius  $r$  according to the phenomenological model of Saitoh et al.<sup>9</sup> is also shown. It is visible from Fig. 5 that the analytical

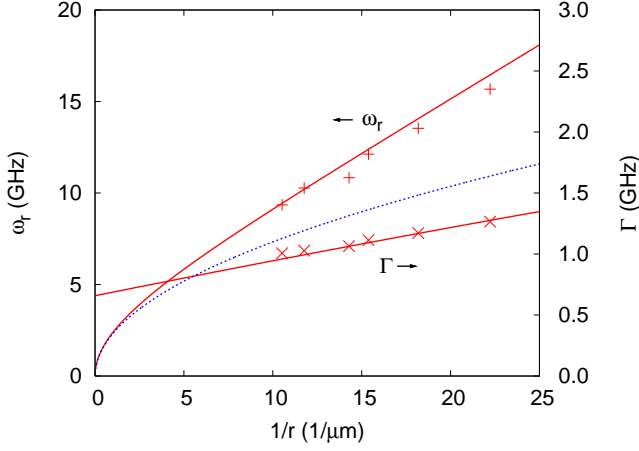


FIG. 5: (Color online) Resonance frequency  $\omega_r$  and damping constant  $\Gamma$  versus reciprocal ring radius. Shown are the values determined from the fits in Fig. 4 (data points) and the analytical values (solid lines). The dashed line indicates the behavior of the resonance frequency as expected from the phenomenological model of Saitoh et al.<sup>9</sup>

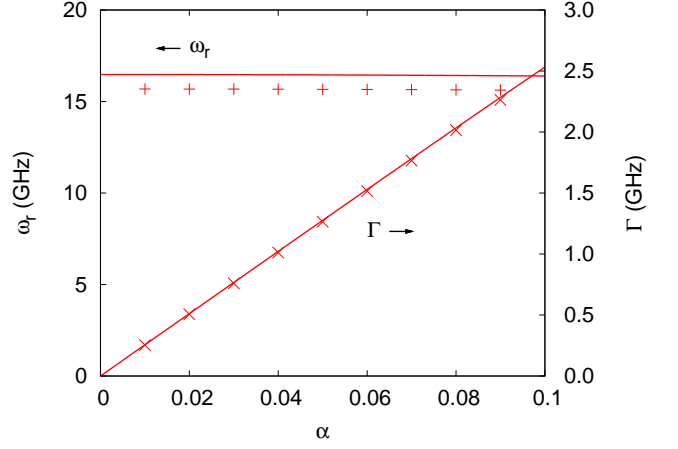


FIG. 7: (Color online) Resonance frequency  $\omega_r$  and damping constant  $\Gamma$  versus Gilbert damping parameter  $\alpha$ . Shown are the values determined from the fits in Fig. 6 (data points) and the analytical values (solid lines).

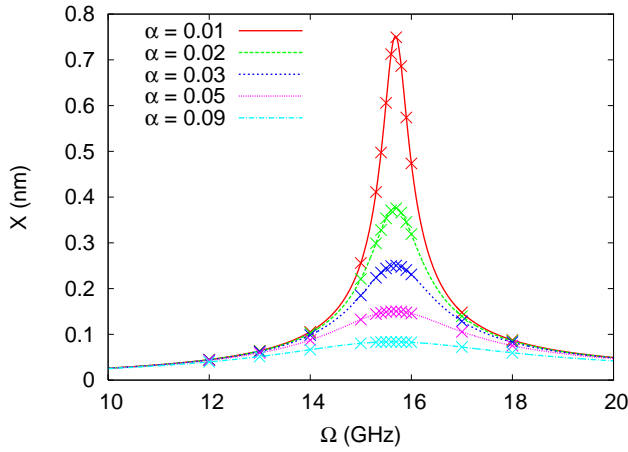


FIG. 6: (Color online) Amplitude of the domain-wall displacement versus frequency of the applied current for different Gilbert damping parameters  $\alpha$ . The ring radius  $r = 45$  nm, the ratio of the exchange and spin-flip relaxation time  $\xi = 0.01$ , and the polarized current density  $j_p = 10^{10}$  A/m<sup>2</sup> are fixed. The crosses denote numerical values while the lines are fits with the analytical result of Eq. (17).

model and the phenomenological oscillator model yield the same eigenfrequencies in the limit of a straight wire ( $r \gg 1 \mu\text{m}$ ). For smaller radii the phenomenological model gives eigenfrequencies which are significantly lower than the ones of the numerical calculations. Our analytical model including the geometrical corrections fits the numerical data very well.

Figures 6 and 7 show the corresponding data for a ring with a radius of 45 nm and different values of the Gilbert damping parameter  $\alpha$ . The analytical solutions are calculated with no free fit parameter. While the data points for the damping constant  $\Gamma(\alpha)$  coincide with the

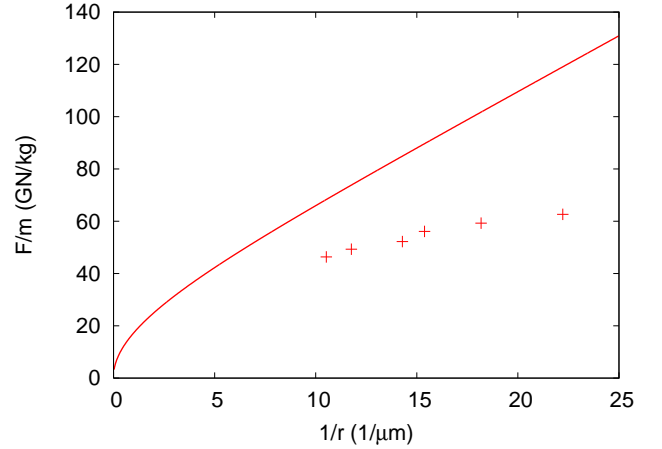


FIG. 8: (Color online) Force per wall mass at the resonance frequency versus reciprocal ring radius. Shown are the numerical values (crosses) and the analytical values (line). The polarized current density is  $j_p = 10^{11}$  A/m<sup>2</sup>.

analytical result, small deviations occur in the resonance frequency  $\omega_r(\alpha)$ . These deviations can be attributed to the finite cell size in our simulations.

In Figs. 8 and 9 the values for the fit parameter  $F(\alpha, r)$  are compared with the analytical result. The analytical values exceed the numerically obtained parameters by up to a factor of two. This difference has several reasons. In Sec. III we assumed that the ground mode can be described by the motion of the center of the wall  $X$  and the magnetization angle  $\phi$ . This neglects spin-wave excitations and higher wall modes. Calculating the mode spectrum excited with a single driving frequency revealed a strong coupling between the ground mode and higher modes. This coupling is enhanced for small radii. Therefore, the force is distributed over several modes, thus decreasing the amplitude of the ground mode. Moreover, in

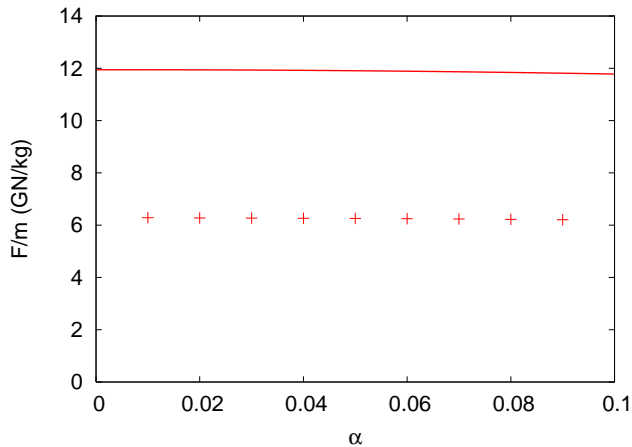


FIG. 9: (Color online) Force per wall mass at the resonance frequency versus Gilbert damping parameter. Shown are the numerical (crosses) and the analytical values (line). The polarized current density is  $j_p = 10^{11}$  A/m<sup>2</sup>.

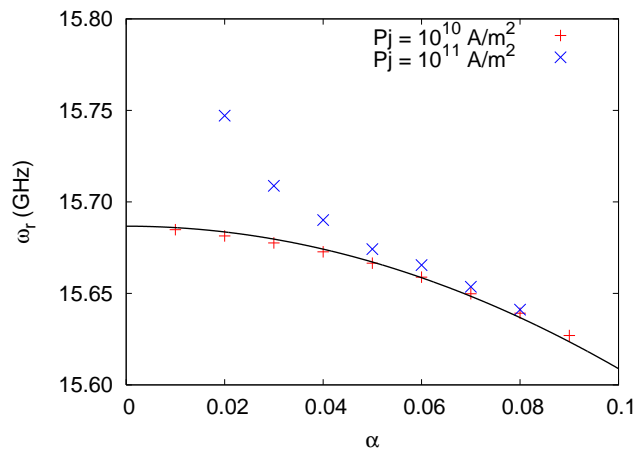


FIG. 10: (Color online) Resonance frequency  $\omega_r$  versus Gilbert damping parameter  $\alpha$ . The data points are the numerical values obtained for a wire with radius 45 nm and two different densities of the polarized current  $j_p$ . The line is a fit according to the analytical result  $\omega_r = C/\sqrt{1 + \alpha^2}$  from Eq. (20) with the fit parameter  $C$ .

wires with small radii the current distribution is very inhomogeneous with a higher current density at their inner edge. We expect that this leads to an additional deformation of the Néel wall. Another aspect is the finite cell size. In the numerical calculations the curved surface has been approximated with rectangular prisms. The resulting kinks in the wire wall have a measurable effect on the domain-wall motion similar to surface roughness.

## VI. RELATION TO EXPERIMENT

In the analytical calculations we assume the linear approximations  $\sin(X/r) \approx X/r$  and  $\sin \phi \approx \phi$ . Nonlin-

earities cause the deviation of the resonance frequency in Fig. 10 from the analytical form at the current density  $j_p = 10^{11}$  A/m<sup>2</sup> and Gilbert damping parameters below 0.05. Note that these non-linearities are small ( $< 0.5\%$ ). The current densities at which non-linearities become important strongly depend on the geometry of the wire. Our analytical model allows to derive them for typical experimental parameters. In the rest of this section we will assume that the damping constant  $\Gamma$  is not field-dependent ( $\frac{\lambda H}{2r} \ll \frac{K_1}{\mu_0 M_s}$ ) and that the squared Gilbert damping parameter is small ( $\alpha^2 \ll 1$ ). These assumptions usually hold in experiments because the domain-wall width  $\lambda$  is small compared to the radius  $r$  and the usual values of the damping parameter  $\alpha$  are lower than 0.1. We can express all terms in Eq. (22) with the expressions for  $\Gamma$  and  $\omega_r$  in Eqs. (18) and (20) when we assume that the ratio of exchange and spin-flip relaxation time  $\xi$  is comparable or less than the Gilbert damping parameter  $\alpha$ . In the case of a non-critically damped oscillation ( $\omega_r > \Gamma$ ) the oscillation becomes nonlinear if the current density is approximately

$$j = \min \left( \frac{\Gamma r}{4b_j}, \frac{\Gamma^2 \lambda}{2\alpha \omega_r b_j} \right). \quad (38)$$

The experimental current densities which Saitoh et al.<sup>9</sup> applied on a wire with cross section  $S = 3150$  nm<sup>2</sup> and radius  $r = 50$   $\mu$ m are well below this current density. They have determined a domain-wall width  $\lambda = 70$  nm, a domain-wall mass  $m = (6.55 \pm 0.06) \cdot 10^{-23}$  kg, and a domain-wall relaxation time  $\tau = \frac{1}{2\Gamma} = (1.4 \pm 0.2) \cdot 10^{-8}$  s. To compare these findings with our analytical model we have to make an assumption for the effective anisotropy constant  $K_{\perp \text{eff}}$ . Assuming the value  $K_{\perp \text{eff}} = 60000 \frac{\text{J}}{\text{m}^3} + \frac{A\pi}{2\lambda r} - \frac{A}{r^2}$  from the fit in Sec. V, Eq. (15) leads to the mass  $m = 1.55 \cdot 10^{-23}$  kg. This mass is comparable to the experimental value, despite the uncertainty of  $K_{\perp \text{eff}}$  due to the different wire dimensions.

As mentioned in Sec. III the analytical calculations lead to relations between the micromagnetic material parameters and the parameters of the harmonic oscillator. These can be used to experimentally determine the Gilbert damping parameter  $\alpha$  from the experimental data. From Eqs. (18), (20), and (15) one can derive the relation

$$\alpha = \frac{2\Gamma\gamma H\lambda}{\omega_r^2 r} = \frac{m\Gamma\gamma\lambda}{\mu_0 M_s S}. \quad (39)$$

With the domain-wall mass and the domain-wall relaxation time of Saitoh's experiment we get a Gilbert damping parameter of  $\alpha = 0.0114 \pm 0.0017$ . This value agrees quite well with the experimental values of Nibarger<sup>47</sup> and Schneider<sup>48</sup> which range from 0.008 to 0.017 for film thicknesses between 10 nm and 93 nm.



## VII. CONCLUSION

The current-induced motion of a domain wall in thin curved nanowires has been investigated. A harmonic-oscillator model which so far had only been introduced phenomenologically is derived from the LLG equations extended by the spin torque according to Zhang and Li.<sup>21</sup> This derivation relates micromagnetic material parameters to the characteristic quantities describing the oscillating domain wall under the influence of an alternating driving current. It is shown that the dipole moment of the wall as well as the curvature of the wire have an important influence on the resonance frequency and damping constant of the oscillation. The domain wall can be seen as a quasi particle in a parabolic potential well which is acted upon by a current-induced force. The phase and magnitude of the force depend on the frequency of the current. The analytical results have been compared to numerical simulations. They agree very well. Our analytical solution suggests new methods to determine material

parameters which are otherwise difficult to measure, e.g., the non-adiabatic term of the spin torque can be determined from the phase shift between the applied current and the overall magnetization. Moreover, the Gilbert damping parameter  $\alpha$  and the domain-wall mass  $m$  follow from a measurement of the resonance frequency  $\omega_r$  and the damping constant  $\Gamma$  of the oscillations.

## Acknowledgments

The authors thank S. S. P. Parkin for sharing his results prior to publication. We appreciate fruitful discussions with U. Gummich. Financial support by the Deutsche Forschungsgemeinschaft via SFB 668 "Magnetismus vom Einzelatom zur Nanostruktur" and via Graduiertenkolleg 1286 "Functional metal-semiconductor hybrid systems" is gratefully acknowledged.

- 
- <sup>1</sup> A. A. Thiele, *J. Appl. Phys.* **45**, 377 (1974).  
<sup>2</sup> N. L. Schreyer and L. R. Walker, *J. Appl. Phys.* **45**, 5406 (1974).  
<sup>3</sup> J. Slonczewski, *J. Magn. Magn. Mater.* **159**, L1 (1996).  
<sup>4</sup> L. Berger, *Phys. Rev. B* **54**, 9353 (1996).  
<sup>5</sup> E. B. Myers, D. C. Ralph, J. A. Katine, R. N. Louie, and R. A. Buhrman, *Science* **285**, 867 (1999).  
<sup>6</sup> J. Grollier, P. Boulenc, V. Cros, A. Hamzi, A. Vaur, A. Fert, and G. Faini, *Appl. Phys. Lett.* **83**, 509 (2003).  
<sup>7</sup> A. Yamaguchi, T. Ono, S. Nasu, K. Miyake, K. Mibu, and T. Shinjo, *Phys. Rev. Lett.* **92**, 077205 (2004).  
<sup>8</sup> H. Koo, C. Krafft, and R. D. Gomez, *Appl. Phys. Lett.* **81**, 862 (2002).  
<sup>9</sup> E. Saitoh, H. Miyajima, T. Yamaoka, and G. Tatara, *Nature* **432**, 203 (2004).  
<sup>10</sup> M. Klauui, C. A. F. Vaz, J. A. C. Bland, W. Wernsdorfer, G. Faini, E. Cambril, and L. J. Heyderman, *Appl. Phys. Lett.* **83**, 105 (2003).  
<sup>11</sup> N. Vernier, D. Allwood, D. Atkinson, M. Cooke, and R. Cowburn, *Europhys. Lett.* **65**, 526 (2004).  
<sup>12</sup> J. A. Katine, F. J. Albert, R. A. Buhrman, E. B. Myers, and D. C. Ralph, *Phys. Rev. Lett.* **84**, 3149 (2000).  
<sup>13</sup> I. N. Krivorotov, N. C. Emley, J. C. Sankey, S. I. Kiselev, D. C. Ralph, and R. A. Buhrman, *Science* **307**, 228 (2005).  
<sup>14</sup> S. S. P. Parkin, US Patent **309**, 6,834,005 (2004).  
<sup>15</sup> D. A. Allwood, G. Xiong, M. D. Cooke, C. C. Faulkner, D. Atkinson, N. Vernier, and R. P. Cowburn, *Science* **296**, 2003 (2002).  
<sup>16</sup> D. A. Allwood, G. Xiong, C. C. Faulkner, D. Atkinson, D. Petit, and R. P. Cowburn, *Science* **309**, 1688 (2005).  
<sup>17</sup> R. P. Cowburn, Patent Application **309**, WO002004077451A1 (2004).  
<sup>18</sup> G. Tatara and H. Kohno, *Phys. Rev. Lett.* **92**, 086601 (2004).  
<sup>19</sup> A. Thiaville, Y. Nakatani, J. Miltat, and Y. Suzuki, *Europhys. Lett.* **69**, 990 (2005).  
<sup>20</sup> X. Waintal and M. Viret, *Europhys. Lett.* **65**, 427 (2004).  
<sup>21</sup> S. Zhang and Z. Li, *Phys. Rev. Lett.* **93**, 127204 (2004).  
<sup>22</sup> S. Zhang and Z. Li, *Phys. Rev. B* **70**, 024417 (2004).  
<sup>23</sup> M. Klauui, C. A. F. Vaz, J. A. C. Bland, W. Wernsdorfer, G. Faini, E. Cambril, L. J. Heyderman, F. Nolting, and U. Ruediger, *Phys. Rev. Lett.* **94**, 106601 (2005).  
<sup>24</sup> T. Ono, H. Miyajima, K. Shigeto, K. Mibu, N. Hosoi, and T. Shinjo, *Science* **284**, 468 (1999).  
<sup>25</sup> Y. Nakatani, A. Thiaville, and J. Miltat, *Nature Materials* **2**, 521 (2003).  
<sup>26</sup> M. Klauui, P.-O. Jubert, R. Allenspach, A. Bischof, J. A. C. Bland, G. Faini, U. Ruediger, C. A. F. Vaz, L. Vila, and C. Vouille, *Phys. Rev. Lett.* **95**, 026601 (2005).  
<sup>27</sup> A. Yamaguchi, S. Nasu, H. Tanigawa, T. Ono, K. Miyake, K. Mibu, and T. Shinjo, *Appl. Phys. Lett.* **86**, 012511 (2005).  
<sup>28</sup> A. Yamaguchi, T. Ono, S. Nasu, K. Miyake, K. Mibu, and T. Shinjo, *Phys. Rev. Lett.* **96**, 179904 (2006).  
<sup>29</sup> J. He, Z. Li, and S. Zhang, *Phys. Rev. B* **73**, 184408 (2006).  
<sup>30</sup> M. Klauui, M. Laufenberg, L. Heyne, D. Backes, U. Ruediger, C. A. F. Vaz, J. A. C. Bland, L. J. Heyderman, S. Cherifi, A. Locatelli, et al., *Appl. Phys. Lett.* **88**, 232507 (2006).  
<sup>31</sup> G. Meier, M. Bolte, R. Eiselt, U. Merkt, B. Krueger, D. Pfannkuche, D. H. Kim, and P. Fischer, unpublished.  
<sup>32</sup> D. Atkinson, D. Allwood, G. Xiong, M. D. Cooke, C. C. Faulkner, and R. P. Cowburn, *Nature Materials* **2**, 85 (2003).  
<sup>33</sup> M. Hayashi, L. Thomas, Y. B. Bazaliy, C. Rettner, R. Moriya, X. Jiang, and S. S. P. Parkin, *Phys. Rev. Lett.* **96**, 197207 (2006).  
<sup>34</sup> L. Thomas, M. Hayashi, R. Moriya, X. Jiang, C. Rettner, and S. S. P. Parkin, *Nature* in press (2006).  
<sup>35</sup> G. Tatara, E. Saitoh, M. Ichimura, and H. Kohno, *Appl. Phys. Lett.* **86**, 232504 (2005).  
<sup>36</sup> R. D. McMichael and M. J. Donahue, *IEEE Trans. Magn.* **33**, 4167 (1997).  
<sup>37</sup> M. Klauui, C. A. F. Vaz, J. A. C. Bland, L. J. Heyderman,

- F. Nolting, A. Pavlovska, E. Bauer, S. Cherifi, S. Heun, and A. Locatelli, *Appl. Phys. Lett.* **85**, 5637 (2004).
- <sup>38</sup> Y. Nakatani, A. Thiaville, and J. Miltat, *J. Magn. Magn. Mater.* **290**, 750 (2005).
- <sup>39</sup> Starting with a high magnetic field the wire is saturated in  $y$ -direction. Reducing the magnetic field to a small offset the system ends up with a domain wall at the bottom of the wire. The wall type depends on the width  $w$  and the thickness  $t$  of the wire<sup>38</sup>. In the present study we choose a small cross section  $S = wt = 100 \text{ nm}^2$  with width  $w = 10 \text{ nm}$  and thickness  $t = 10 \text{ nm}$  to get a transverse wall.
- <sup>40</sup> L. Landau and E. Lifshitz, *Physik. Z. Sowjetunion* **8**, 153 (1935).
- <sup>41</sup> Uniaxial anisotropy can be taken into account by replacing the anisotropy constants  $K$  and  $K_{\perp\text{eff}}$  with the new constants  $K'$  and  $K'_{\perp}$  given by  $K' = \bar{K} + K_y - K_x$  and  $K'_{\perp} = K_{\perp\text{eff}} + K_z - K_y$ .
- <sup>42</sup> V. K. Dugaev, V. R. Vieira, P. D. Sacramento, J. Barnaś, M. A. N. Araújo, and J. Berakdar, *Phys. Rev. B* **74**, 054403 (2006).
- <sup>43</sup> **OOMMF User's Guide, Version 1.0** M.J. Donahue and D.G. Porter Interagency Report **NISTIR 6376**, National Institute of Standards and Technology, Gaithersburg, MD (Sept 1999) (<http://math.nist.gov/oommf/>).
- <sup>44</sup> J. Cash and A. Karp, *ACM Trans. Math. Softw.* **16**, 201 (1990).
- <sup>45</sup> R. D. McMichael and M. D. Stiles, *J. Appl. Phys.* **97**, 10J901 (2005).
- <sup>46</sup> M. Bolte, G. Meier, and C. Bayer, *Phys. Rev. B* **73**, 052406 (2006).
- <sup>47</sup> J. Nibarger, R. Lopusnik, and T. Silva, *Appl. Phys. Lett.* **82**, 2112 (2003).
- <sup>48</sup> M. Schneider, T. Gerrits, A. Kos, and T. Silva, *Appl. Phys. Lett.* **87**, 072509 (2005).